Inorg. Chem. **2008**, *47*, 10866−10874

Magnetostructural Relationship in the Spin-Crossover Complex t-{Fe(abpt)$_2$[N(CN)$_2$]$_2$}: Polymorphism and Disorder Phenomenon

Chou-Fu Sheu,[†] Sébastien Pillet,*[,‡] Yen-Chen Lin,[†] Szu-Miao Chen,[†] I-Jui Hsu,[†] Claude Lecomte,[‡] and Yu Wang*[,†]

Department of Chemistry, National Taiwan University, Taipei, 10617 Taiwan, and LCM3B, UMR CNRS 7036, Nancy-Université, BP 239, 54506 Vandoeuvre-les-Nancy, France

Received May 14, 2008

t-{Fe(abpt)$_2$[N(CN)$_2$]$_2$} [abpt = 4-amino-3,5-bis(pyridin-2-yl)-1,2,4-triazole] is an intriguing spin-crossover system that crystallizes in two polymorphs. Polymorph **A** is paramagnetic; its crystal structure consists of a single molecule located at the center of inversion symmetry. Polymorph **B**, on the other hand, exhibits a rather complicated two-step-like spin transition; its crystal structure consists of two symmetry-independent molecules. The crystal structure of polymorph **B** has been derived in the different spin states: above the high-temperature step (300 K), between the two steps (90 K), below the incomplete low-temperature step (50 K), in the light-induced metastable state (15 K), in the thermally quenched metastable state (15 K), and after relaxation from the quenched state (15 K). The correlation between the structure and magnetic properties is precisely established, allowing the complicated magnetic behavior of polymorph **B** to be well understood. A unique order−disorder phase transition, resulting in a modulation of the metastable state structures, is detected for the first time on such spin-transition compounds. The modulation of the structure originates from a particular ordering of the dicyanamide ligand at one of the two Fe sites.

Introduction

Octahedrally coordinated transition-metal complexes with a $3d^4-3d^7$ electronic configuration may exhibit different spin states, namely, high-spin (HS) or low-spin (LS) states, depending on the ligand-field strength exerted on the metal ion. Under certain conditions, the spin-crossover (SCO) phenomena were found in some of these complexes, where the spin state can be fine-tuned by external perturbations, such as variation in the temperature or pressure, or by counterions or even with solvent molecule exchange. Light irradiation is another efficient way to induce the spin transition; the light-induced excited spin-state trapping (LIESST)[1] and reverse-LIESST[2] effects in the solid state have been intensively studied in recent years. A few reviews[3] give extensive and thorough discussions on all of the possible factors that could affect the SCO behavior. The characteristics in the magnetic property of such spin transitions are intimately related to the cooperativity of the molecular crystal lattice.[4] Even for a mononuclear system, the elastic interactions, associated with the large change in molecular volume during spin transition, can effectively spread out by intermolecular contacts, such as hydrogen-bonding or aromatic $\pi-\pi$ interactions.[5] Highly cooperative materials often exhibit abrupt spin transition, sometimes accompanied with thermal hysteresis, which is particularly attractive for potential applications in molecular sensing, molecular switching, data storage, display, and other electronic devices.[6] Quite often the spin transition occurs together with a structural phase transition (order−disorder transition, for instance), especially for a two-step or multistep transition;[7] for instance, the two-step spin transition of [Fe(2-pic)$_3$]Cl$_2$·EtOH (2-pic = 2-picolylamine) has been attributed to the onset of an interme-

* To whom correspondence should be addressed. E-mail:sebastien.pillet@lcm3b.uhp-nancy.fr (S.P.), wangyu@ntu.edu.tw (Y.W.).
[†] National Taiwan University.
[‡] Nancy-Université.

(1) (a) Decurtins, S.; Gütlich, P.; Köhler, C. P.; Spiering, H.; Hauser, A. *Chem. Phys. Lett.* **1984**, *105*, 1–4. (b) Decurtins, S.; Gütlich, P.; Hasselbach, K. M.; Hauser, A.; Spiering, H. *Inorg. Chem.* **1985**, *24*, 2174–2178. (c) Gütlich, P.; Hauser, A. *Coord. Chem. Rev.* **1990**, *97*, 1–22.
(2) (a) Hauser, A. *Chem. Phys. Lett.* **1986**, *124*, 543–548. (b) Hauser, A. *J. Chem. Phys.* **1991**, *94*, 2741–2748.
(3) (a) Real, J. A.; Gaspar, A. B.; Muñoz, M. C. *Dalton Trans.* **2005**, 2062–2079. (b) Gütlich, P.; Hauser, A.; Spiering, H. *Angew. Chem., Int. Ed. Engl.* **1994**, *33*, 2024–2054. (c) *Topics in Current Chemistry*; Gütlich, P., Goodwin, H. A., Eds.; Springer-Verlag: Berlin, 2004; Vols. *233− 235*.
(4) Real, J. A.; Gaspara, A. B.; Niel, V.; Muñoz, M. C. *Coord. Chem. Rev.* **2003**, *236*, 121–141.

10.1021/ic800879c CCC: $40.75
Published on Web 10/29/2008

diate superstructure phase, coupled to two successive order−disorder phase transitions.[8] Such a multistep behavior normally involves more than one unique site for metal ions.[9] Spinlike domains were observed, by means of single-crystal diffraction experiments, for either the thermal or photoinduced SCO in some highly cooperative materials.[8b,10] The change in the coordination geometry due to the spin transition is quite significant; the typical difference in the $Fe-N_{ligand}$ bond length between HS and LS species is 0.2 Å for iron(II) complexes; the distortion of the octahedron, defined as Σ[11] and Θ,[12] is much higher in the HS state than in the LS state. Therefore, the characterization of the structural reorganization during the spin transition is crucial for the understanding of the corresponding magnetic behavior. The effect of polymorphism upon SCO behavior was known for a long time; one of the best examples is the $[Fe(PM\text{-}BiA)_2(NCS)_2]$ complex [PM-BiA = (*N*-2-pyridylmethylene)-4-aminobiphenyl], which exhibits, depending on the synthetic method, an abrupt spin transition (phase I) with a very narrow hysteresis or a gradual spin conversion (phase II).[13] $Fe[(p\text{-}IC_6H_4)B(3\text{-}Mepz)_3]_2$[14] (3-Mepz = 3-methylpyrazolyl) as well as other $FeL_2(NCX)_2$ examples with L = bt (bt = 2,2′-bi-2-thiazoline) (X = S)[15] or L = abpt [abpt = 4-amino-3,5-bis(pyridin-2-yl)-1,2,4-triazole] (X = S, Se)[16] were found in which one polymorph displays SCO behavior but the other polymorph remains paramagnetic. In the case of $FeL(NCS)_2$, L = (3-aminopropyl)bis(2-pyridylmethyl)amine,[17] there exist three polymorphs with magnetic properties different from one another. Polymorph **A** undergoes a gradual spin transition (T_C = 176 K) without hysteresis, polymorph **B** is paramagnetic over 4.5−295 K, whereas polymorph **C** exhibits a very abrupt spin transition with a hysteresis of 8 K.[17] A recent work[18] on $[Fe(2\text{-}pic)_3]Cl_2$ with 2-propanol solvate in the lattice showed clearly that the interplay between the spin conversion and the order−disorder phenomenon of the solvent molecule is the reason for the complicated magnetic behavior. Therefore, detail structural information at various temperatures and conditions (thermally quenched or light-induced excitation) is crucial for the understanding of the corresponding magnetic behavior. According to the structural results on the $[Fe^{II}L_n(NCS)_2]$ series, the distortion of the metal coordination sphere appears to be linearly correlated with the *T*(LIESST) value.[19] The lifetime of the metastable HS state relies mainly on the coordination sphere[20] rather than on the cooperativity. Unfortunately, up to now, only a handful of single-crystal structures have been determined in the LIESST metastable state.[8b,21] t-$\{Fe(abpt)_2[N(CN)_2]_2\}$ is a SCO system that was first investigated by Moliner et al.[22] The rather unusual magnetic behavior after normal cooling and thermally quenched treatments was quite interesting but could not be correlated well with the structure reported. In addition, an almost quantitative LIESST effect with an extremely slow relaxation rate below 20 K makes it a good candidate for structure investigation at the metastable state.

We report in this paper the existence of two polymorphs for the title compound: one is identical with those reported by Moliner et al.[22] (**A** hereafter); the other is a new polymorph (**B** hereafter). The temperature-dependent magnetic properties indicate a paramagnetic species for **A** and a very complicated behavior for **B**, in fact the same as that

(5) (a) Létard, J.-F.; Guionneau, P.; Rabardel, L.; Howard, J. A. K.; Goeta, A. E.; Chasseau, D.; Kahn, O. *Inorg. Chem.* **1998**, *37*, 4432–4441. (b) Boca, R.; Boca, M.; Dlhan, L.; Falk, K.; Fuess, H.; Haase, W.; Jarosciak, R.; Papankova, B.; Renz, F.; Vrbova, M.; Werner, R. *Inorg. Chem.* **2001**, *40*, 3025–3033. (c) Létard, J.-F.; Guionneau, P.; Codjovi, E.; Lavastre, O.; Bravic, G.; Chasseau, D.; Kahn, O. *J. Am. Chem. Soc.* **1997**, *119*, 10861–10862. (d) Halcrow, M. A. *Polyhedron* **2007**, *26* (14), 3523–3576. (e) Boca, R.; Renz, F.; Boca, M.; Fuess, H.; Haase, W.; Kickelbick, G.; Linert, W.; Vrbova-Schikora, M. *Inorg. Chem. Commun.* **2005**, *8* (2), 227–230. (f) Brefuel, N.; Imatomi, S.; Torigoe, H.; Hagiwara, H.; Shova, S.; Meunier, J.-F.; Bonhommeau, S.; Tuchagues, J.-P.; Matsumoto, N. *Inorg. Chem.* **2006**, *45*, 8126–8135. (g) Matouzenko, G. S.; Bousseksou, A.; Borshch, S. A.; Perrin, M.; Zein, S.; Salmon, L.; Molnar, G.; Lecocq, S. *Inorg. Chem.* **2004**, *43*, 227–236. (h) Holland, J. M.; McAllister, J. A.; Lu, Z.; Kilner, C. A.; Thornton-Pett, M.; Halcrow, M. A. *Chem. Commun.* **2001**, 577–578.

(6) (a) Létard, J.-F.; Guionneau, P.; Goux-Capes, L. *Top. Curr. Chem.* **2004**, *235*, 221–249. (b) Kahn, O.; Kröber, J.; Jay, C. *Adv. Mater.* **1992**, *4*, 718–728. (c) Kahn, O.; Martinez, C. J. *Science* **1998**, *279*, 44–48. (d) Kahn, O. *Chem. Br.* **1999**, *35* (2), 24–27. (e) Renz, F.; de Souza, P. A.; Klingelhöfer, G.; Goodwin, H. A. *Hyperfine Interact.* **2002**, *139/140*, 699–704. (f) Bousseksou, A.; Molnar, G. C. R. *Chimie* **2003**, *6*, 1175–1183. (g) Varret, F.; Bleuzen, A.; Boukheddaden, K.; Bousseksou, A.; Codjovi, E.; Enachescu, C.; Goujon, A.; Linares, J.; Menendez, N.; Verdaguer, M. *Pure Appl. Chem.* **2002**, *74* (11), 2159–2168.

(7) (a) Matouzenko, G. S.; Luneau, D.; Molnár, G.; Ould-Moussa, N.; Zein, S.; Borshch, S. A.; Bousseksou, A.; Averseng, F. *Eur. J. Inorg. Chem.* **2006**, *13*, 2671–2682. (b) Ortega-Villar, N.; Thompson, A. L.; Muñoz, M. C.; Ugalde-Saldívar, V. M.; Goeta, A. E.; Moreno-Esparza, R.; Real, J. A. *Chem.—Eur. J.* **2005**, *11* (19), 5721–5734. (c) Boinnard, D.; Bousseksou, A.; Dworkin, A.; Savariault, J. M.; Varret, F.; Tuchagues, J. P. *Inorg. Chem.* **1994**, *33*, 271–281.

(8) (a) Chernyshov, D.; Hostettler, M.; Törnroos, K. W.; Bürgi, H.-B. *Angew. Chem., Int. Ed.* **2003**, *42*, 3825–3830. (b) Huby, N.; Guérin, L.; Collet, E.; Toupet, L.; Ameline, J. C.; Cailleau, H.; Roisnel, T.; Tayagaki, T.; Tanaka, K. *Phys. Rev. B* **2004**, *69*, 020101(R)

(9) (a) Garcia, Y.; Kahn, O.; Rabardel, L.; Chansou, B.; Salmon, L.; Tuchagues, J. P. *Inorg. Chem.* **1999**, *38*, 4663–4670. (b) Hibbs, W.; Arif, A. M.; van Koningsbruggen, P. J.; Miller, J. S. *CrystEngComm* **1999**, *1*, 12–14. (c) Hibbs, W.; van Koningsbruggen, P. J.; Arif, A. M.; Shum, W. W.; Miller, J. S. *Inorg. Chem.* **2003**, *42*, 5645–5653.

(10) (a) Pillet, S.; Hubsch, J.; Lecomte, C. *Eur. Phys. J. B* **2004**, *38*, 541–552. (b) Pillet, S.; Legrand, V.; Souhassou, M.; Lecomte, C. *Phys. Rev. B* **2006**, *74*, 140101(R). (c) Guionneau, P.; Le Gac, F.; Lakhoufi, S.; Kaiba, A.; Chasseau, D.; Létard, J.-F.; Négrier, P.; Mondieig, D.; Howard, J. A. K.; Léger, J.-M. *J. Phys.: Condens. Matter* **2007**, *19*, 326211.

(11) Guionneau, P.; Marchivie, M.; Bravic, G.; Létard, J.-F.; Chasseau, D. *J. Mater. Chem.* **2002**, *12*, 2546–2551.

(12) Marchivie, M.; Guionneau, P.; Létard, J.-F.; Chasseau, D. *Acta Crystallogr.* **2005**, *B61*, 25–28.

(13) Létard, J.-F.; Chastanet, G.; Nguyen, O.; Marcen, S.; Marchivie, M.; Guionneau, P.; Chasseau, D.; Gütlich, P. *Monatsh. Chem.* **2003**, *134*, 165–182.

(14) Reger, D. L.; Gardinier, J. R.; Smith, M. D.; Shahin, A. M.; Long, G. J.; Rebbouh, L.; Grandjean, F. *Inorg. Chem.* **2005**, *44*, 1852–1866.

(15) Ozarowski, A.; McGarvey, B. R.; Sarkar, A. B.; Drake, J. E. *Inorg. Chem.* **1988**, *27*, 628–635.

(16) (a) Moliner, N.; Muñoz, M. C.; Létard, S.; Létard, J.-F.; Solans, X.; Burriel, R.; Castro, M.; Kahn, O.; Real, J. A. *Inorg. Chim. Acta* **1999**, *291*, 279–288. (b) Gaspar, A. B.; Muñoz, M. C.; Moliner, N.; Ksenofontov, V.; Levchenko, G.; Gütlich, P.; Real, J. A. *Monatsh. Chem.* **2003**, *134*, 285–294.

(17) Matouzenko, G. S.; Bousseksou, A.; Lecocq, S.; van Koningsbruggen, P. J.; Perrin, M.; Kahn, O.; Collet, A. *Inorg. Chem.* **1997**, *36*, 5869–5879.

(18) Törnroos, K. W.; Hostettler, M.; Chernyshov, D.; Vangdal, B.; Bürgi, H.-B. *Chem.—Eur. J.* **2006**, *12*, 6207–6215.

(19) Guionneau, P.; Marchivie, M.; Bravic, G.; Létard, J.-F.; Chasseau, D. *Top. Curr. Chem.* **2004**, *234*, 97–128.

(20) (a) Létard, J.-F. *J. Mater. Chem.* **2006**, *16*, 2550–2559. (b) Létard, J.-F.; Guionneau, P.; Nguyen, O.; Costa, J. S.; Marcén, S.; Chastanet, G.; Marchivie, M.; Goux-Capes, L. *Chem.—Eur. J.* **2005**, *11*, 4582–4589.

given by the earlier report.[22] The crystal structures of this new polymorph **B** at various temperatures, at the thermally quenched as well as the LIESST metastable states, are described in order to establish the magnetostructural relationship. A unique order−disorder phase transition involving a modulation of the crystal structure is also observed for the first time in spin-transition compounds.

Experimental Section

Synthesis. $FeSO_4 \cdot 7H_2O$, sodium dicyanamide [$NaN(CN)_2$], and abpt were purchased and used as received without further purification. Both polymorphs of the title compound were synthesized following an adaptation of the procedure given in the literature.[22]Single crystals, suitable for X-ray analyses, were grown using a slow diffusion method in a test tube: a methanol/water (1:1) solution (10 mL) of abpt (0.02 mmol) was layered on top of a water solution (10 mL) containing stoichiometric amounts of $NaN(CN)_2$ and $FeSO_4 \cdot 7H_2O$, with a small amount of ascorbic acid (1 mg) added to prevent the oxidation of iron(II). After 1 week, orange crystal aggregates formed on the wall of the tube and were extracted by filtering. By careful examination of the crystal aggregates with an optical microscope, it appeared that two polymorphs with different crystal morphology coexisted in the batch. The longer well-shaped prism crystals (**A**) could be easily distinguished from the smaller cubiclike crystals (**B**); the photographs of the crystals in two polymorphs are shown in Figure 1. Crystals of both polymorphs for magnetic and diffraction measurements were manually separated under the microscope.

Magnetic Measurements. The temperature-dependent magnetic susceptibility was measured using a Quantum Design SQUID magnetometer (MPMS-XL7) operating at 0.2 T and the temperature range of 2−300 K. Experimental susceptibilities were corrected for diamagnetism of the constituent atoms by using the Pascal's constants.[23] After careful separation of polymorphs **A** and **B** under a microscope, the variable-temperature magnetic susceptibility measurements were carried out separately for **A** and **B** on small crystals in the cooling and warming modes at a rate of 2 K/min. For thermal quenching measurements, the sample was rapidly cooled to 5 K by sliding the sample into the SQUID measuring chamber, which is held at 5 K and then warmed slowly following the procedure described in the literature.[22]

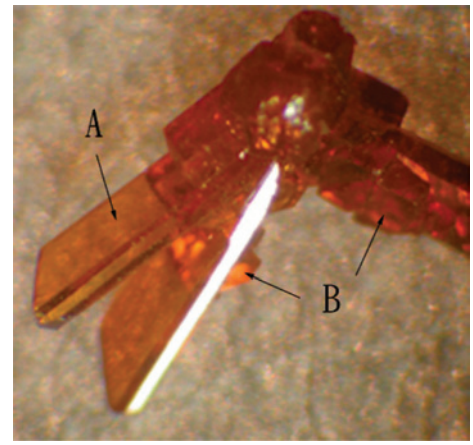

Figure 1. Photograph of a crystal aggregate containing both **A** and **B** polymorphs.

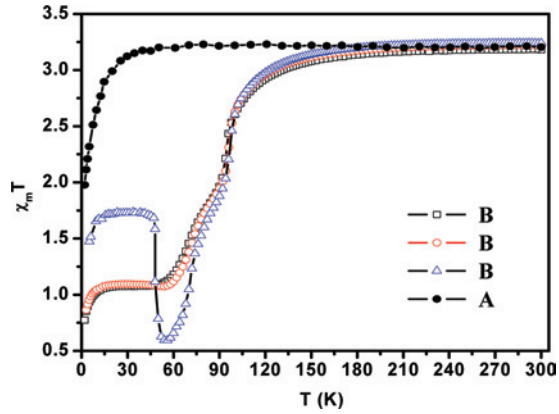

Figure 2. Temperature dependence of $\chi_m T$ for polymorphs **A** (solid) and **B** (open). For **B**, the open squares and circles represent the normal cooling and warming modes, respectively, and the thermal quenching measurement (open triangles) was performed in the warming mode from 5 K.

X-ray Crystallography. In order to thoroughly describe the thermo- and photomagnetic properties and relate these to the crystal structures of polymorph **B**, three data sets were collected at 300, 90, and 50 K (along the thermal spin transition) and three others at 15 K in the thermally quenched metastable, relaxed (see below), and photoinduced metastable states. The 15 K quenched crystal structure was derived from data collected on the BM01A beamline at the ESRF with a wavelength of 0.710 Å, equipped with a MAR345 area detector. The 50 K data were measured on a Bruker-Kappa CCD machine equipped with a Helix cryosystem (Oxford Cryosystem), whereas an Oxford Diffraction Xcalibur diffractometer equipped with a Sapphire 2 CCD detector was used to collect all other data sets. The Oxford Diffraction liquid-N_2 and Helijet systems were used for the 90 and 15 K data collections, respectively.

The 15 K thermally quenched metastable state was obtained by rapidly introducing the crystal, beforehand centered on the goniometer head, into the cooling He gas stream on the diffractometer. The "relaxed" form was obtained by slow warming from the quenched state to 56 K, which corresponds to the minimum on the $\chi_m T$ vs T curve (Figure 2), kept there for 3 h before further cooling to 15 K, at which the "relaxed" form data were collected. The photoexcited diffraction experiment was carried out by exposing the crystal prepared in the "relaxed" form to the 534 nm line of an Ar−Kr gas laser for 4 min (P = 40 mW) at 15 K. Subsequent lattice parameter determination confirmed the occurrence of complete LS to HS photoconversion, by comparison with the lattice parameters determined for the thermally quenched state.

(21) (a) Kusz, J.; Spiering, H.; Gütlich, P. *J. Appl. Crystallogr.* **2000**, *33*, 201–205. (b) Kusz, J.; Spiering, H.; Gütlich, P. *J. Appl. Crystallogr.* **2001**, *34*, 229–238. (c) Kusz, J.; Schollmeyer, D.; Spiering, H.; Gütlich, P. *J. Appl. Crystallogr.* **2005**, *38*, 528–536. (d) Marchivie, M.; Guionneau, P.; Howard, J. A. K.; Chastanet, G.; Létard, J.-F.; Goeta, A. E.; Chasseau, D. *J. Am. Chem. Soc.* **2002**, *124*, 194–195. (e) Thompson, A. L.; Goeta, A. E.; Real, J. A.; Galet, A.; Muñoz., M. C. *Chem. Commun.* **2004**, 1390–1391. (f) Niel, V.; Thompson, A. L.; Goeta, A. E.; Enachescu, C.; Hauser, A.; Galet, A.; Muñoz, M. C.; Real, J. A. *Chem.—Eur. J.* **2005**, *11*, 2047–2060. (g) Ichiyanagi, K.; Hebert, J.; Toupet, L.; Cailleau, H.; Guionneau, P.; Létard, J.-F.; Collet, E. *Phys. Rev. B* **2006**, *73*, 060408(R). (h) Money, V. A.; Evans, I. R.; Halcow, M. A.; Goeta, A. E.; Howard, J. A. K. *Chem. Commun.* **2003**, 158–159. (i) Money, V. A.; Elhaïk, J.; Halcow, M. A.; Howard, J. A. K. *Dalton Trans.* **2004**, 1516–1518. (j) MacLean, E. J.; McGrath, C. M.; O'Connor, C. J.; Sangregorio, C.; Seddon, J. M. W.; Sinn, E.; Sowrey, F. E.; Teat, S. J.; Terry, A. E.; Vaughan, G. B. M.; Young, N. A. *Chem.—Eur. J.* **2003**, *9*, 5314–5322. (k) Legrand, V.; Pillet, S.; Weber, H.-P.; Souhassou, M.; Létard, J.-F.; Guionneau, P.; Lecomte, C. *J. Appl. Crystallogr.* **2007**, *40*, 1076–1088. (l) Trzop, E.; Buron-Le Cointe, M.; Cailleau, H.; Toupet, L.; Molnar, G.; Bousseksou, A.; Gaspar, A. B.; Real, J. A.; Collet, E. *J. Appl. Crystallogr.* **2007**, *40*, 158–164.

(22) Moliner, N.; Gaspar, A. B.; Munõz, M. C.; Niel, V.; Cano, J.; Real, J. A. *Inorg. Chem.* **2001**, *40*, 3986–3991.

(23) Mulay, L. N.; Boudreaux, E. A. *Theory and Application of Molecular Diamagnetism*; Wiley-Interscience: New York, 1976.

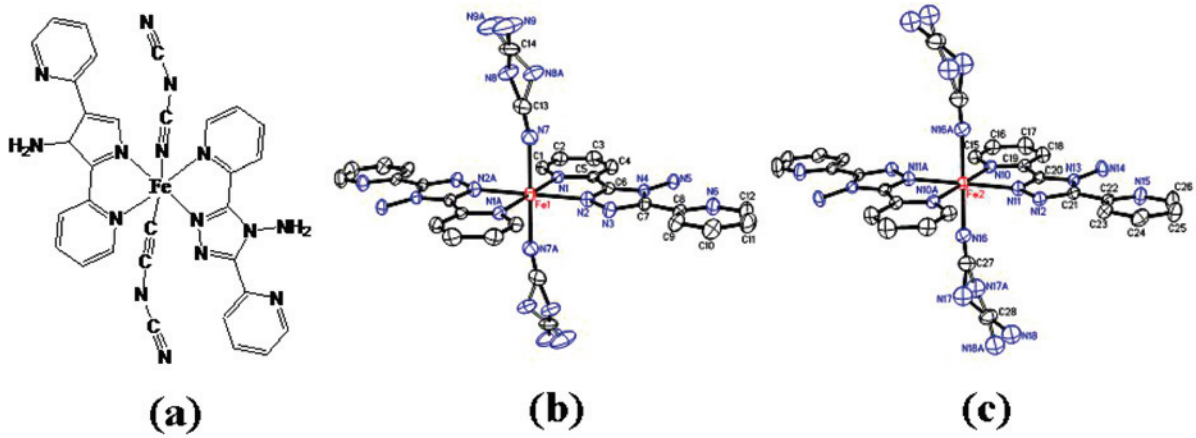

Figure 3. (a) Structural line drawing of the molecule. ORTEP drawings with 30% probability ellipsoid and atomic labeling for polymorph **B** at 300 K. The solid and open bonds on $[N(CN)_2]^-$ represent the two disordered positions at (b) Fe1 and (c) Fe2.

Table 1. Crystal Data and Structure Refinement of t-{$Fe(abpt)_2[N(CN)_2]_2$} in Polymorphs **A** and **B**

	polymorph **A**[22]	polymorph **B**					
	293 K	300 K	90 K	50 K	15 K (quenched)	15 K (relaxed)	15 K (light induced)
cryst syst	triclinic	triclinic	triclinic	triclinic	triclinic	triclinic	triclinic
space group	$P\bar{1}$	$P\bar{1}$	$P\bar{1}$	$P\bar{1}$	$P\bar{1}$	$P\bar{1}$	$P\bar{1}$
a (Å)	8.4618(5)	9.599(2)	9.202(1)	9.351(1)	9.545(1)	9.248(1)	9.6395(9)
b (Å)	9.6086(3)	9.989(2)	10.019(1)	9.825(1)	9.854(1)	9.786(2)	9.821(2)
c (Å)	9.6381(7)	16.106(2)	16.041(2)	15.975(2)	15.817(2)	16.132(3)	15.738(3)
α (deg)	83.661(4)	97.724(13)	96.498(9)	97.601(3)	97.69(1)	97.65(1)	97.745(1)
β (deg)	86.642(5)	102.270(14)	100.932(9)	101.936(3)	101.92(1)	101.56(1)	102.057(1)
γ (deg)	65.821(4)	92.256(13)	94.820(9)	92.929(2)	92.23(1)	93.33(1)	91.816(1)
V (Å^3)	710.44(7)	1491.6(4)	1434.4(4)	1418.7(2)	1439.1(3)	1412.2(4)	1441.1(4)
Z	1	2	2	2	2	2	2
$\sin(\theta)/\lambda_{max}$ (Å^{-1})	0.62	0.68	0.73	0.77	0.60	0.74	0.71
measd reflns	2993	14 028	13 440	18 511	8462	11 630	8101
indep reflns	2795	8489	8180	6251	4545	5805	7099
ave redundancy	1.1	1.7	1.6	3.0	1.9	1.5	1.1
completeness (%)	100	86.3	86.6	95.7	88.4	78.8	84.2
R(int)	0.015	0.060	0.079	0.098	0.017	0.043	0.096
R1 [$I > 2\sigma(I)$]	0.034	0.065	0.065	0.069	0.065	0.085	0.068

The nozzle of the liquid-He cryosystems we used prohibits part of the moving space of the goniometer, which makes data completeness difficult to reach for the triclinic system. However, data completeness of over 90% has been reached to a maximum resolution of $2\theta_{max} = 50°$ for the data sets collected at 15 and 50 K. For the remaining data sets, the completeness at $2\theta_{max} = 50°$ is over 99.5%. Anyhow, as checked, the structural parameters obtained including data up to $2\theta_{max} = 50°$, on the one hand, and those obtained including data up to the highest resolution, on the other hand, give the same results. The only appreciable difference is in the thermal parameters, which, as expected, are lower when the higher resolution data are included. Therefore, reflections of higher resolution were always included in the refinement, at the expense of the data completeness.

The Bragg intensities of the 50 K data set were integrated by using *EVALCCD*,[24] and the absorption corrections were applied using *SADABS*.[25] For all of the other data sets, the diffraction frames were integrated using *CRYSALIS*,[26] and numerical absorption corrections were applied based on the indexed crystal faces. In all cases, intensities were merged in the $P\bar{1}$ space group using SORTAV.[27]

The structures were solved by direct methods and refined with full-matrix least squares based on F^2 using *SHELXS*[28] and *SHELXL*,[29] respectively. All non-hydrogen atoms were refined anisotropically, and hydrogen atoms were located in difference Fourier maps and refined isotropically. Difference Fourier maps also evidenced heavy orientational disorder of the $N(CN)_2$ moiety on both molecules for all of the structures, with the exception of the Fe1 molecule in the two metastable phases (see below). This disorder was taken into account during the structural refinements using two positions for the dycianamide ligands and related fragment population parameters. Restraints on the anisotropic displacement parameters of the disordered dicyanamide parts were applied when necessary. Details on the experiments and crystal data are given in Table 1.

Results

Syntheses and Characterization of the Two Polymorphs. The smaller crystals, attributed to polymorph **B**, did show a color

(24) (a) Duisenberg, A. J. M. Reflections on Area Detectors. Ph.D. Thesis, Utrecht University, Utrecht, The Netherlands, 1998. (b) Duisenberg, A. J. M.; Kroon-Batenburg, L. M. J.; Schreurs, A. M. M. *J. Appl. Crystallogr.* **2003**, *36*, 220–229.

(25) Sheldrick, G. M. *SADABS*, version 2.03; University of Göttingen: Göttingen, Germany, 2002.

(26) *CrysAlis CCD and CrysAlis RED*, version 1.171; Oxford Diffraction: Wroclaw, Poland, 2004.

(27) (a) Blessing, R. H. *Acta Crystallogr.* **1995**, *A51*, 33–37. (b) Blessing, R. H. *J. Appl. Crystallogr.* **1989**, *22*, 396–397.

(28) Sheldrick, G. M. *SHELXS97, Program for Structure Solution*; University of Göttingen: Göttingen, Germany, 1997.

(29) (a) Sheldrick, G. M. *SHELXL97, Program for Structure Refinement*; University of Göttingen: Göttingen, Germany, 1997. (b) Macrae, C. F.; Edgington, P. R.; McCabe, P.; Pidcock, E.; Shields, G. P.; Taylor, R.; Towler, M.; van de Streek, J. *J. Appl. Crystallogr.* **2006**, *39*, 453–457.

change from orange to black under the liquid-N_2 stream, while the big ones (phase **A**) did not show any change under the same condition. For iron(II) SCO compounds with pyridyl-type ligands, the metal-to-ligand charge-transfer band is expected to be more intense in the LS state because of the shorter metal−ligand bond length, which would result in a better overlap between the metal and ligand orbitals as compared to the HS state.[30] The observed color change suggests that **B** may undergo spin transition and that the liquid-N_2 temperature is below the transition temperature. For each polymorph, several single crystals were preliminarily characterized by X-ray diffraction at room temperature. **A** was confirmed to be identical with that reported in the literature,[22] while **B** exhibited different cell constants with respect to **A**. The existence of two polymorphs was therefore firmly established.

Magnetic Properties. The temperature-dependent $\chi_m T$ values of **A** and **B** polymorphs in the temperature range 2−300 K are shown in Figure 2. The $\chi_m T$ value of 3.20 cm^3 K mol^{-1} for **A** at 300 K is within the range of expected value for a paramagnetic iron(II) in its HS state with some orbital contributions. The magnetic measurement clearly indicates that the iron in **A** remains in its HS state in the temperature range studied. The drop of $\chi_m T$ below 40 K may be a consequence of zero-field splitting (ZFS) of iron(II) in the HS state.

On the contrary, a rather complicated magnetic behavior is observed for **B**, which is very close to that of the earlier report on the **A** structure,[22] and presumably the earlier $\chi_m T$ measurements were made on a sample containing mostly the **B** form. According to the magnetic measurement shown in Figure 2, a $\chi_m T$ value of 3.19 cm^3 K mol^{-1} at 300 K is observed; when cooling at the normal rate, the value decreased to 2.0 cm^3 K mol^{-1} at 90 K and then gradually decreased to 1.09 cm^3 K mol^{-1} at 56 K, where it stayed as a plateau until 15 K, before taking another drop to 0.75 cm^3 K mol^{-1} at 2 K. However, for the thermally quenched sample, it started with 1.48 cm^3 K mol^{-1} at 5 K, increased quite abruptly to 1.73 cm^3 K mol^{-1} at 15 K, and stayed constant until 50 K, before it took an abrupt drop to 0.60 cm^3 K mol^{-1} at 56 K; such a state (called the "relaxed state" here) can only be obtained by warming up the thermally quenched sample from 15 to 56 K. By further cooling to lower temperature (15 K) from this point, the $\chi_m T$ value would remain constant at 0.60 cm^3 K mol^{-1}. A detailed description of such magnetic behaviors was given in the earlier paper;[22] the LIESST phenomenon is also expected to be the same.

Crystal Structures of Polymorph B Relative to Polymorph A. In view of the complex magnetic behavior of t-{$Fe(abpt)_2[N(CN)_2]_2$} and to go beyond the interpretation, six accurate crystal structures of polymorph **B** have been derived as a function of the temperature and the sample history in the different spin states: (i) through the thermal spin transition by slow cooling (300, 90, and 50 K), (ii) after thermal quenching in the thermally induced excited spin state transition (TIESST, 15 K), (iii) after subsequent relaxation from the thermally quenched state (15 K), and (iv) in the LIESST (15 K). Detailed structural descriptions at various states will be given and compared to the structure reported by Moliner et al.[22] (polymorph **A**). The crystal data and brief outlines of the refinements at various states are given in Table 1.

All structures of polymorph **B** can be described in the same space group $P\bar{1}$ with a common triclinic unit cell [a = 9.599(2) Å, b = 9.989(2) Å, c = 16.106(2) Å, α = 97.724(13)°, β = 102.270(14)°, γ = 92.256(13)°, V = 1491.6(4) $Å^3$, Z = 2, at 300 K]. The asymmetric unit consists of the halves of t-{$Fe(abpt)_2[N(CN)_2]_2$} molecular entities, located on two independent inversion centers, (0, 0, $^1/_2$) for molecule 1 (Fe1) and (0, 0, 0) for molecule 2 (Fe2). Each iron atom is octahedrally coordinated by two abpt ligands and two $[N(CN)_2]^-$ anions in trans fashion, shown in Figure 3a. Owing to intermolecular interactions, the dicyanamide ligands are differently oriented with respect to the equatorial abpt ligand in both molecules; they are, furthermore, disordered over two orientations, as indicated in parts b and c of Figure 3, respectively, with occupancies of 0.75/0.25 and 0.63/0.37 for Fe1 and Fe2, respectively, at 300 K. This disorder is one of the main structural features of polymorph **B** and undergoes a remarkable transition to incommensurate order in the metastable state (thermally quenched and light induced).

The geometrical characteristics of the [FeN_6] octahedra are listed in Table 2. The Fe−N(pyridyl) bond distance is slightly longer than the Fe−N(triazole) and Fe−N(dicyanamide) ones. This inequivalence is similar to those of related SCO complexes containing bidentate abpt ligands,[5g,31a] including **A**,[22] and results in elongated and distorted [FeN_6] octahedra, as can be judged by the large angular distortion parameters Σ and Θ. Altogether, the Fe−N bond lengths, angular distortion parameters, and polyhedral volumes are very similar for Fe1 and Fe2 and are consistent with both iron atoms in the HS configuration at room temperature.[19] The amino groups of the abpt ligands form intraligand short hydrogen bonds with the uncoordinated pyridyl nitrogen [N5···N6 = 2.851(5) Å and N14···N15 = 2.827(5) Å at 300 K]; these hydrogen bonds contribute to the nearly planar configuration of the abpt ligand, as reported for all other mononuclear abpt complexes.[16,22,31] Accordingly, this affords an almost planar geometry of the equatorial coordination. The dihedral angles between the uncoordinated pyridyl and the triazole moieties are 5.5(2)° and 7.2(1)° for Fe1 and Fe2, respectively.

The crystal packing consists of two sublattices, (1) and (2), that form alternating layers stacked along the c axis, as illustrated in Figure 4. The lattice parameters a and b represent the intralayer Fe···Fe distances, whereas c/2

(30) Hauser, A. *Top. Curr. Chem.* **2004**, *234*, 155–198.

(31) (a) Kunkeler, P. J.; van Köningsbruggen, P. J.; Cornelissen, J. P.; van der Horst, A. N.; van der Kraan, A. M.; Spek, A. L.; Haasnoot, J. G.; Reedijk, J. *J. Am. Chem. Soc.* **1996**, *118*, 2190–2197. (b) Faulmann, C.; van Köningsbruggen, P. J.; de Graaff, R. A. G.; Haasnoot, J. G.; Reedijk, J. *Acta Crystallogr.* **1990**, *C46*, 2357–2360. (c) Cornelissen, J. P.; van Diemen, J. H.; Groeneveld, L. R.; Haasnoot, J. G.; Spek, A. L.; Reedijk, J. *Inorg. Chem.* **1992**, *31*, 198–202. (d) van Königsbruggen, P. J.; Goubitz, K.; Haasnoot, J. G.; Reedijk, J. *Inorg. Chim. Acta* **1998**, *268*, 37–42.

Table 2. FeN_6 Octahedral Geometry in Different Spin States for t-{$Fe(abpt)_2[N(CN)_2]_2$}

T (K)	site	assigned spin state	Fe−N(py) (Å)	Fe−N(trz) (Å)	Fe−N(dicyan) (Å)	Σ^a (deg)	Θ^b (deg)	$V_p{}^c$ (Å^3)
				Polymorph **A**[22]				
293		HS	2.216(2)	2.121(2)	2.160(2)	64.0	273.4	13.1
				Polymorph **B**				
300	Fe1	HS	2.203(3)	2.139(3)	2.138(3)	64.0	265.3	13.0
	Fe2	HS	2.200(3)	2.141(3)	2.106(3)	67.6	269.4	12.8
90	Fe1	LS	2.014(3)	1.978(3)	1.959(2)	44.6	181.5	10.3
	Fe2	HS	2.195(3)	2.141(3)	2.109(2)	65.4	266.7	12.8
50	Fe1	LS	2.038(3)	1.997(3)	1.984(2)	49.6	194.4	10.6
	Fe2	Mix	2.106(3)	2.064(3)	2.049(4)	57.4	225.9	11.6
15, quenched	Fe1	HS	2.170(3)	2.102(3)	2.112(2)	58.4	248.5	12.5
	Fe2	HS	2.182(3)	2.128(3)	2.126(3)	66.6	253.8	12.8
15, relaxed	Fe1	LS	2.005(4)	1.981(4)	1.962(3)	47.5	184.9	10.2
	Fe2	Mix	2.075(4)	2.031(4)	1.992(3)	50.7	210.4	11.0
15, LIESST	Fe1	HS	2.203(3)	2.150(2)	2.129(3)	63.5	268.2	13.1
	Fe2	HS	2.195(3)	2.141(3)	2.145(4)	70.4	267.0	13.0

[a] Distortion parameters Σ, defined as the sum of the absolute values of the deviation from 90°, of the 12 cis angles in the coordination sphere. [b] Distortion parameters Θ, defined as the sum of the deviations from 60°, of the 24 possible θ angles. [c] Volume V_p of the FeN_6 octahedron.

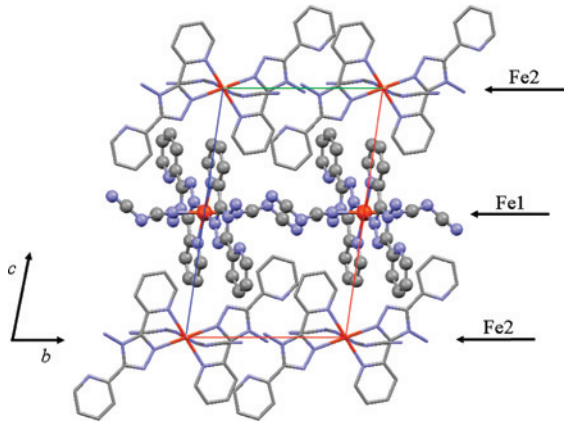

Figure 4. Crystal structure of polymorph **B**, consisting of alternating layers Fe1 and Fe2 stacked along the *c* axis. The disorder of $[N(CN)_2]^-$ is omitted for clarity.

corresponds to the interlayer spacing. The structural topology of each sublattice is analogous to each other, as well as the intermolecular contacts. As depicted in Figure 5, each a sublattice is built from 1D molecular chains running along *a* and *b* for (1) and (2), respectively, connected by intermolecular $\pi\cdots\pi$ interactions between neighboring parallel abpt planes. Such a chain stacking is rather usual for abpt complexes and has already been reported for the isostructural $[Fe(abpt)_2(NCS)_2]$ and $[Fe(abpt)_2(NCSe)_2]$ systems[16a] and the polymorph **A** of t-{$Fe(abpt)_2[N(CN)_2]_2$}. As shown in Table 3, the $\pi\cdots\pi$ stacking interaction for layers (1) is stronger than that for layers (2), which is, in turn, slightly stronger than for that for **A**: at room temperature, the distances between the nearest abpt plane are 3.600, 3.555(9), and 3.459(5) Å respectively for **A** and sublattices (2) and (1) of **B**. Adjacent chains are further connected by short nonlinear N···H−N hydrogen bonds between the terminal nitrogen of the axial dicyanamide ligand and one hydrogen of the amino group (N5 and N14) of neighboring abpt ligands. Such an interaction [N···N = 2.901(9) Å at 300 K] is one of the strongest observed for similar dicyanamide···amino connections (on 75 occurrences in the CSD). Each sublattice is further stabilized by a network of C−H···N weak hydrogen bonds. Short repulsive N···N contacts (less than 3 Å) occur between two neighboring dicyanamide groups of Fe2 and may be responsible for the observed structural disorder.

Structural Reorganization upon the Thermal Spin Transition (T = 300, 90, and 50 K). Upon a gradual lowering of the temperature from 300 to 50 K, the magnetic measurements indicate a gradual spin transition with a shoulder at 90 K. Accordingly, we undertook a comparative structural analysis at 300, 90, and 50 K, whose results are given here. At room temperature, Fe−N distances and distortion parameters are similar for both Fe1 and Fe2 molecules and are consistent with a HS−HS configuration. By lowering of the temperature to 90 K, the Fe1 coordination polyhedron becomes more regular, while the Fe1−N distances decrease by ∼0.2 Å, leading to a ∼3 Å^3 polyhedral volume decrease. These changes are as expected for a HS-to-LS molecular conversion. On the contrary, the Fe2 coordination polyhedron remains almost unchanged with respect to 300 K. By a further decrease of the temperature to 50 K, the Fe2 polyhedron undergoes a global contraction (by 0.8 Å^3) and Fe−N bond shortening, intermediate between the room temperature values and those observed for Fe1. It is to be noted that the occupancies of the two disorder configurations of the dicyanamide ligands are dependent on the temperature, as listed in Table 3, and as one might anticipate to the molecular spin state. As a matter of fact, the disorder of the Fe1 molecule decreases with a lowering of the temperature from 300 to 50 K.

Crystal Structures of the TIESST and "Relaxed" States at 15 K. In order to achieve an efficient TIESST process, a single crystal was rapidly inserted into the liquid-He stream at 15 K, with the thermal equilibrium within the crystal being reached within a few seconds under such conditions.[32] The corresponding diffraction pattern exhibits extra features with respect to those recorded at room temperature. In addition to the Bragg peaks, satellite reflections have been observed and indexed using four reciprocal basis vectors (**a***, **b***, **c***, and **q**). The derived **q** vector ($\mathbf{q}_{quenched} = 0.338(5)\mathbf{a}^* + 0.557(6)\mathbf{b}^* - 0.047(5)\mathbf{c}^*$) indicates

(32) (a) Teng, T.-Y.; Moffat, K. *J. Appl. Crystallogr.* **1998**, *31*, 252–257. (b) Walker, L. J.; Moreno, P. O.; Hope, H. *J. Appl. Crystallogr.* **1998**, *31*, 954–956.

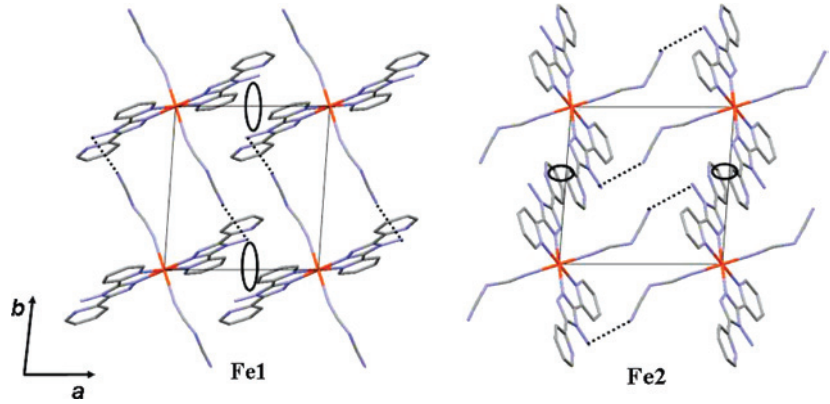

Figure 5. Molecular packing within sublattices (1) and (2) in polymorph **B**. The dotted lines and black ellipsoids represent the short intermolecular hydrogen-bond and $\pi\cdots\pi$ interactions, respectively. The disorder of $[N(CN)_2]^-$ is omitted for clarity.

Table 3. Intra- and Interligand Hydrogen Bonds (Å) and Dihedral Angles (deg) within abpt in the Different Spin States and Disorder Fractions of the Dicyanamide Ligand

T (K)	site	intraligand hydrogen bond[a]	dihedral angle[b]	$\pi\cdots\pi$ stacking distance (Å)	interligand hydrogen bond[c]	disorder fraction
			Polymorph **A**			
293[22]	Fe1	2.896(3)	8.3(1)	3.600	3.126	ordered
			Polymorph **B**			
300	Fe1	2.851(5)	5.5(2)	3.459(5)	2.96(1), 2.82(3)	0.75/0.25
	Fe2	2.827(5)	7.2(1)	3.555(9)	2.90(1), 3.04(1)	0.63/0.37
90	Fe1	2.840(5)	2.2(2)	3.343(5)	2.89(1), 3.2(1)	0.90/0.10
	Fe2	2.831(4)	9.8(1)	3.453(8)	2.91(1), 2.96(1)	0.45/0.55
50	Fe1	2.842(5)	4.1(2)	3.334(4)	2.92(2), 2.9(2)	0.91/0.09
	Fe2	2.820(5)	10.0(1)	3.426(9)	2.87(1), 3.13(2)	0.70/0.30
15, quenched	Fe1	2.845(4)	5.1(1)	3.335(4)	2.926(4)	ordered
	Fe2	2.820(4)	8.4(1)	3.458(6)	2.86(1), 3.17(1)	0.62/0.38
15, relaxed	Fe1	2.833(6)	3.4(2)	3.327(5)	2.92(4), 2.9(1)	0.77/0.23
	Fe2	2.837(6)	9.4(1)	3.412(10)	2.90(1), 3.15(3)	0.84/0.16
15, LIESST	Fe1	2.844(4)	5.7(1)	3.335(4)	2.922(4)	ordered
	Fe2	2.807(5)	8.4(1)	3.478(8)	2.86(1), 3.15(1)	0.60/0.40

[a] Distance between the nitrogen atom of the amino group and the uncoordinated pyridyl ring $[N(NH_2)\cdots N(pyridyl)]$. [b] Dihedral angle between the triazole ring and the uncoordinated pyridyl ring in abpt. [c] Distance between the nitrogen atom of the amino group and the neighboring dicyanamide ligand $[N(NH_2)\cdots N(CN)_2]$.

that the corresponding crystal structure is incommensurably modulated. We report here only the structural analysis based on the central Bragg peaks, neglecting in a first approach the contribution from the satellite reflections; the reported crystal structure corresponds, therefore, to the average structure. The complete description of the incommensurate phase and its relation to the magnetic properties will be discussed in a forthcoming paper. The crystal data and the FeN_6 coordination geometry for the average structure are listed in Tables 1 and 2.

By thermal quenching to 15 K, a complete ordering of the dicyanamide ligand of Fe1 occurs, while the disorder for Fe2 is retained. For both molecules, the Fe−N bond lengths, angular distortion parameters, and polyhedral volume are close but smaller than those characterized at room temperature.

In order to obtain the crystal structure of the "relaxed" form after the thermally quenched state, the crystal was gradually warmed up to 56 K, while the evolution of the lattice parameters was monitored as a function of the temperature. Around 50−56 K, a sudden decrease of the unit cell volume indicates that a HS-to-LS thermally activated relaxation occurs. Meanwhile, the satellite peaks disappear around 50 K. The crystal was then kept at 56 K for 3 h to ensure the completeness (saturation) of the relaxation before the crystal was cooled down to 15 K, where the data for the "relaxed" form were measured. The corresponding unit cell volume is the smallest listed in Table 1. The Fe1−N bond lengths are slightly shorter than those derived at 50 K, while the polyhedral volumes nearly match. For Fe2, the structural characteristics differ significantly from the 50 K case, with much shorter Fe2−N distances, smaller polyhedral volumes, and angular distortion parameters. Interestingly, the dicyanamide disorder is retrieved for Fe1.

Crystal Structure of the LIESST Metastable State. The LIESST metastable state was produced by 534 nm laser light exposure during 4 min on a single-crystal sample prepared beforehand in the "relaxed" form at 15 K, as described above. As for the TIESST state, the diffraction pattern indicates an incommensurate modulation of the crystal structure ($\mathbf{q}_{photoinduced} = 0.331(2)\mathbf{a}^* + 0.658(2)\mathbf{b}^* - 0.000(3)\mathbf{c}^*$); we restrict ourselves to the average structure in the present context. The LIESST state crystal structure exhibits significant differences with respect to the TIESST metastable state. For both Fe1 and Fe2, an elongation of the Fe−N coordination bond, together with an increase in the angular distortion parameters and polyhedral volumes, arises. Such a difference most prob-

ably results from a slight relaxation occurring during the thermal quenching procedure. The molecular structure of Fe1 is completely ordered, as is the case in the thermally quenched state.

Discussion

Comparison of the Magnetic Properties of Polymorphs A and B. Polymorphism in SCO systems with different magnetic properties was known in many cases[15−17] and often possibly attributed to dissimilar crystal packings in different polymorphs, which could as a consequence perturb the FeN_6 coordination sphere. However, a direct elucidation of the spin-transition properties from a careful structural analysis is a difficult task because, in general, subtle changes in intermolecular interactions may result in radically different transition behaviors. In the present situation, polymorphic differences in the crystal packing are detected, as listed in Table 3. Both **A** and **B** exhibit, as a first approximation, a 1D chain structural organization with, nonetheless, shorter $\pi\cdots\pi$ distances between abpt ligands for **B**. The main differences in the crystal packing originate from the presence of short intermolecular hydrogen bonds between the nitrogen of the uncoordinated cyano group of $[N(CN)_2]^-$ and the amino group of abpt in **B**, whereas C···C contacts are responsible for the chain packing in **A**. These differences may be partly responsible for the different magnetic behavior. According to the similar topology of each sublattice in **B**, the shift of 24 K in the transition temperature is probably due to the subtle difference between the Fe1 and Fe2 coordination spheres, such as the smaller dihedral angle between the triazole ring and the uncoordinated pyridyl ring, the slightly longer intraligand N···H−N hydrogen bond of abpt, and the slightly shorter $\pi-\pi$ interaction distance between adjacent abpt ligands around Fe1 (Table 3). Furthermore, short N···N contacts between adjacent $[N(CN)_2]^-$ occur only in the sublattice of Fe2.

Polymorph **A** consists of paramagnetic HS molecular entities in the whole temperature range studied (2−300 K). Of course, the existence of two crystallographic independent sites in **B** explains well the two-step-like spin-transition behavior, which is attributed to the HS-to-LS conversion of the two iron sites at slightly different temperatures.[9] On the basis of our structural findings and especially the distinct structural features at 90 and 50 K for Fe1 and Fe2, the spin transition at ∼94 K corresponds to Fe1, while the transition at 70 K accounts for Fe2. A linear relationship is found between the bond distance of Fe−N and Θ.

Magnetostructural Relationship at the Thermal Spin-State Transition. On the basis of past experiences on the change in FeN_6 octahedral geometry as a function of the iron(II) spin state,[33] it is reliable to assess the spin state from the Fe−N bond length and the extent of distortion from a regular octahedron. Typical HS/LS differences in the Fe−N bond length amount to ∼0.2 Å, while a decrease of the octahedron volume (V_p) from about 13 to 10 Å^3 is usually reported.[19] Spin-state assignments of the two iron sites are summarized in Table 2. It is apparent that the spin states deduced from the Fe−N bond lengths are consistent with the magnetic measurements given in Figure 2. Both Fe1 and Fe2 are in the HS configuration at 300 K corresponding to a $\chi_m T$ value of 3.19 cm^3 K mol^{-1}. When cooling to 90 K, Fe2 remains in the HS state whereas Fe1 undergoes a complete transition to LS. The $\chi_m T$ value of 2.00 cm^3 K mol^{-1} at this temperature is somewhat larger than expected for such a LS−HS case. While repeating the crystal structure at 90 K using various 300−90 K cooling rates, we did observe, in some cases, mixed spin states on both Fe1 and Fe2 sites judging from the Fe−N distance and distortion parameters. Kinetic effects are certainly effective here as reported for other SCO systems;[34] the cooling rate is a very delicate and key controlling factor in the present situation. Upon a further decrease of the temperature to 50 K, Fe2 turns to a mixed spin state, where neither the bond length nor distortion values are decisive; even the Fe1 center is not so conclusive, with a slightly longer Fe−N bond length and a larger distortion than was expected for a purely LS case; the $\chi_m T$ value, 1.09 cm^3 K mol^{-1}, corresponds to about two-thirds of the HS residue on one Fe site, attributed mainly to Fe2.

Magnetostructural Relationship in the Metastable States. All of the structural data indicate that the thermally quenched metastable state corresponds to the status that both Fe sites are at the HS state, but the magnetic measurements ($\chi_m T$ value of 1.70 cm^3 K mol^{-1}) correspond to the status that only half of the Fe sites are at the HS state. This disagreement may result from the differences in the quenching processes. While the tiny single crystal can be quenched within a few seconds[32] for the diffraction measurements, it takes, on the other hand, at least 5 min to reach thermal equilibrium for the SQUID measurements. Expectedly, a higher HS trapping is achieved in the diffraction experiment. A close inspection of the Fe−N bond distances in the quenched metastable state points to slightly shorter values than those obtained at room temperature. Accordingly, a minor HS-to-LS relaxation during the quenching procedure might be effective.

Warming from this quenched state, the magnetic moment first increases to reach a plateau until 56 K, where a sudden drop takes place, which corresponds to a ∼19% residual HS species; T_{TIESST} is characterized at 56 K in agreement with Moliner et al.[22] The FeN_6 coordination geometry at 15 K after relaxation indicates that Fe1 is in the LS state, while Fe2 presents nearly one-third of the residual HS species, in fair agreement with the magnetic results. From the structural analysis, the HS residual species are localized essentially on site Fe2.

Although we did not measure the magnetic moment corresponding to the LIESST state, we believe it should behave exactly the same as that reported earlier.[22] The $\chi_m T$ value of 2.9 cm^3 K mol^{-1} at 38 K[22] indicated that all Fe

(33) Alvarez, S. *J. Am. Chem. Soc.* **2003**, *125*, 6795–6802.

(34) (a) Ritter, G.; König, E.; Irler, W.; Goodwin, H. A. *Inorg. Chem.* **1978**, *17*, 224–228. (b) Grunert, C. M.; Goodwin, H. A.; Carbonera, C.; Létard, J.-F.; Kusz, J.; Gütlich, P. *J. Phys. Chem. B* **2007**, *111*, 6738–6747.

ions are at HS, taking into account the ZFS effect at low temperature. Sure enough, the FeN_6 geometry for this LIESST metastable state (Table 2) confirms that both Fe1 and Fe2 are in their HS states based on the Fe−N bond lengths and distortion parameters.

Disorder to Incommensurate Order Transition in the Metastable States. As introduced above, the diffraction patterns of the thermally quenched and light-induced metastable states present satellite reflections, related to a modulation of the crystal structure. The average structures of the TIESST and LIESST metastable states both indicate a complete ordered configuration of the dicyanamide group attached to Fe1, while $[N(CN)_2]^-$ coordinated to Fe2 undergoes an incommensurate ordering. At the relaxation temperatures T_{TIESST} and T_{LIESST}, parallel to the HS-to-LS structural reorganization, the structural disorder reemerges on both iron sites. This unique disorder to incommensurate order transition is observed for the first time by thermal quenching and light-induced excitation.

Prethermal-Treatment-Dependent Ground States at 56 K. Apparently **B** attains different thermodynamic ground states depending on the previous thermal treatment. When cooling from 300 to 56 K at a normal rate, the $\chi_m T$ value corresponds to LS at Fe1 and approximately two-thirds of the HS residue at Fe2; while warming from low temperature to 56 K of the thermally quenched species, the $\chi_m T$ value corresponds to LS at Fe1 and approximately one-third of the HS residue at Fe2. The phenomenon can now be elucidated on the basis of our structural results. Not only are the HS crystal structures of 300 K and of those thermally quenched at 15 K different because of the singular modulation structure of the metastable HS state, but also the spin transition procedures are not the same for the two processes. When the temperature is decreased from 300 K, an intermediate state, comprising alternate HS and LS layers along the *c* axis, will be reached first. As for warming the thermally quenched sample, the relaxation from HS to LS happens either simultaneously or stepwise at the two iron sites. The relaxation rate at both iron sites is expected to be different because of the different thermal transition temperature (94 K on Fe1 and 70 K on Fe2); theoretically, the rate of relaxation at Fe2 would be slower than that of Fe1 because of the lower transition temperature.[30] This can explain why the HS residue is always located at Fe2.

Conclusion

t-{$Fe(abpt)_2[N(CN)_2]_2$} presents two polymorphs that display different behaviors in magnetic properties. Polymorph **A**, as described by Moliner et al.,[22] consists of a single molecular species; the temperature-dependent magnetic curve indicates a paramagnetic property with a $\chi_m T$ value as expected for iron(II) at the HS state. On the contrary, in polymorph **B**, two independent molecular entities are found in the crystal that form alternating layers of molecules along the crystallographic *c* axis. The structure−magnetic property relationship is established in such a way that at room temperature both iron sites are at the HS state, whereas decreasing the temperature to 90 K induces first the complete HS-to-LS conversion of Fe1 site and further decreasing the temperature to 50 K only induces the partial HS-to-LS conversion ($\sim^1/_3$) of the Fe2 site. By light irradiation or thermal quenching, a metastable state was obtained at very low temperature; the corresponding crystal structures at 15 K indicate that both iron sites are at the HS state for the LIESST case, while a small fraction of the LS state developed during the thermal quenching procedure. The disorder in the dicyanamide ligand at the Fe1 site disappears in both metastable states. The presence of satellite peaks on the diffraction patterns of both of these metastable states indicates a modulation of the crystal structure; the modulation persists until the HS-to-LS relaxation temperature is around 56 K, indicating that the modulation of the crystal structure and the HS metastable state are closely related to each other. With the structures investigated at various temperatures and in the thermally quenched and light-induced metastable states, the relationship between the structure and magnetic properties can be precisely established. The complicated behavior of the magnetic properties of polymorph **B** is therefore completely understood.

Acknowledgment. We thank the National Science Council of the Republic of China and CNRS of France for support of this work. The NSC/CNRS and NSC/FIT orchid collaboration projects are highly appreciated.

Supporting Information Available: Crystallographic data in CIF format for the polymorph **B** under various conditions. This material is available free of charge via the Internet at http://pubs.acs.org. A total of six CIF files have been deposited as CCDC 687118−687123 with the Cambridge Crystallographic Data Centre. These files can be obtained, on request, from the Director, Cambridge Crystallographic Data Centre, 12 Union Road, Cambridge, CB2 1EZ, U.K.

IC800879C